Balancing fluorescence and singlet oxygen formation in push-pull type near-infrared BODIPY photosensitizers

Jasper Deckers,[a,b]† Tom Cardeynaels,[a,b,c]† Sandra Doria,[d,e] Nikolay Tumanov,[f] Andrea Lapini,[d,g] Anitha Ethirajan,[b,h] Marcel Ameloot,[i] Johan Wouters,[f] Mariangela Di Donato,[d,e] Benoît Champagne,[c] Wouter Maes[a,b]*

[a] UHasselt – Hasselt University, Institute for Materials Research (IMO), Design & Synthesis of Organic Semiconductors (DSOS), Agoralaan, 3590 Diepenbeek, Belgium
[b] IMEC, Associated Lab IMOMEC, Wetenschapspark 1, 3590 Diepenbeek, Belgium
[c] UNamur – University of Namur, Namur Institute of Structured Matter, Theoretical and Structural Physical Chemistry Unit, Laboratory of Theoretical Chemistry (LTC), Rue de Bruxelles 61, 5000 Namur, Belgium
[d] European Laboratory for Non-Linear Spectroscopy (LENS), Via Nello Carrara 1, 50019 Sesto Fiorentino (FI), Italy
[e] Instituto di Chimica dei Composti OrganoMetallici (ICCOM-CNR), Via Madonna Del Piano 10, 50019 Sesto Fiorentino (FI), Italy
[f] UNamur – University of Namur, Namur Medicine and Drug Innovation Center (NAMEDIC), Namur Research Institute for Life Sciences (NARILIS), Namur Institute of Structured Matter (NISM), Rue de Bruxelles 61, 5000 Namur, Belgium
[g] Department of Chemistry, Life Science and Environmental Sustainability, University of Parma, Parco Area delle Scienze, 17/A, 43124 Parma, Italy
[h] UHasselt – Hasselt University, Institute for Materials Research (IMO), Nano-Biophysics and Soft Matter Interfaces (NSI), Wetenschapspark 1, 3590 Diepenbeek, Belgium
[i] UHasselt – Hasselt University, Biomedical Research Institute (BIOMED), Agoralaan, 3590 Diepenbeek, Belgium

† These authors contributed equally.
* wouter.maes@uhasselt.be

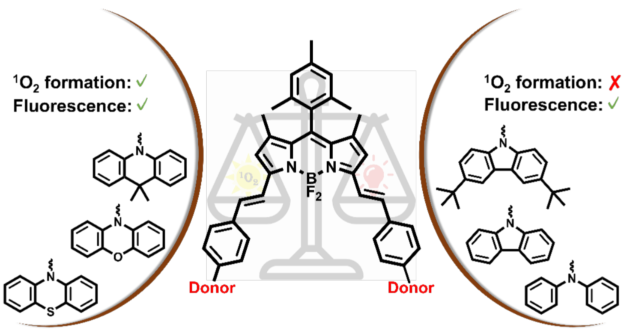

Abstract

Boron dipyrromethene dyes are highly attractive for image-guided photodynamic therapy. Nevertheless, their clinical breakthrough as theranostic agents is still obstructed by several limitations. Here, we report a series of strongly absorbing, heavy-atom-free, distyryl-BODIPY donor-acceptor dyads operating within the phototherapeutic window. Whereas diphenylamine and carbazole donors lead to strong fluorescence, dimethylacridine, phenoxazine, and phenothiazine units afford a decent fluorescence combined with the efficient formation of singlet oxygen. Dedicated photophysical analysis and quantum-chemical calculations are performed to elucidate the excited state dynamics responsible for the pronounced differences within the BODIPY series. Femtosecond transient absorption spectra reveal the nature of the excited state processes and the involvement of charge-transfer states in triplet formation.

Introduction

Singlet oxygen (denoted as $O_2(^1\Delta_g)$ or shortly $^1O_2$) is a powerful reagent that is employed in the manufacture of fine chemicals, wastewater treatment, blood sterilization, and the production of specific insecticides and herbicides, among others.[1] Furthermore, the combination of its high reactivity, related short lifetime, and slow diffusion rate in biological media, renders $^1O_2$ the protagonist in photodynamic therapy (PDT).[2, 3] In PDT, light is used to activate a photosensitizer (PS), which then produces reactive oxygen species (ROS) through different mechanisms.[4] These ROS result in the selective destruction of tumor cells at the irradiation site, allowing PDT to be used for cancer therapy. Furthermore, PDT can also be employed in a broader sense for treating ophthalmic and dermatologic diseases, bacterial and fungal infections, and the inactivation of viruses.[5-12] Whereas type I PDT investigates ROS formation upon direct interaction of the activated PS with a substrate, most studies focus on the type II PDT process since $^1O_2$ is considered the leading cytotoxic agent.[13] In more detail, in this process the PS is excited with photons of a suitable wavelength, thereby achieving an electronically excited singlet state (S_n). For $^1O_2$ formation, intersystem crossing (ISC) is required to obtain a triplet state (T_n) from which energy transfer to molecular oxygen ($O_2(^3\Sigma_g^-)$ or $^3O_2$) can occur.[14] As ISC is a spin-forbidden transition, the quest for compounds with efficient triplet formation remains a crucial research topic.

Throughout the years, a vast amount of organic photosensitizers have been reported.[15-23] Among these promising molecules, 4,4-difluoro-4-bora-3*a*,4*a*-diaza-*s*-indacenes (commonly indicated as boron dipyrromethenes or BODIPYs) are one of the most prominent examples.[24-36] Their high molar extinction coefficients, (photo)chemical stability, and easily tunable photophysical properties make them attractive PSs.[37-39] However, typically high fluorescence quantum yields (Φ_f) of BODIPY dyes imply ISC restrictions as these are competing decay processes for the first singlet excited state. The most encountered solution is the introduction of bromine, iodine, or transition metal complexes on the BODIPY structure, thereby increasing spin-orbit coupling (SOC) through the so-called heavy-atom effect.[40-43] Nevertheless, related additional synthetic efforts and costs, shortened triplet state lifetimes, low photostability, and increased dark cytotoxicity provided an impetus to search for alternative ISC mechanisms.[44-46] In this way, novel BODIPY PSs were developed, based on reduced singlet-triplet energy gaps (ΔE_{ST}), spin converters, radical-enhanced ISC, radical pair ISC, twisted π-conjugation-induced ISC, and spin-orbit charge-transfer ISC (SOCT-ISC).[40-42, 47, 48] These alternative approaches open the possibility for theranostic applications as subtle engineering of the energy levels can allow triplet population and singlet emission to coexist. In PDT, these self-reporting PSs present an appealing step toward personalized cancer treatment, enabling the combination of diagnosis and therapy to localize the target, monitor the therapeutic progression, and improve drug dosimetry.[49-51]

Another essential feature for PDT PSs is their activity in the near-infrared (NIR) spectral region. Shorter wavelengths are more prone to scattering and several tissue chromophores will filter the UV-VIS part of the incoming light.[14, 52, 53] Wavelengths between 600 and 800 nm are desired to limit light scattering, reduce background signals, and enhance tissue penetration depths.[54] Although strategies to bathochromically shift the absorption and emission properties are well-known for BODIPY dyes, it is not straightforward to combine strong $^1O_2$ production with a decent brightness in the phototherapeutic region.[55-58] Hence, only a handful of NIR-photoactive heavy-atom-free dual-functioning BODIPY PSs have been developed so far.[59-65,66]

Recently, we reported a series of distyryl-BODIPY-acridine dyads, active in the phototherapeutic window, showing balanced brightness and phototoxic power.[66] Concentration-dependent fluorescence experiments suggested the involvement of 'exciplex'[67] energy states in the decay mechanism. Relatively long exciplex state lifetimes, combined with their polar nature, would render them a suitable intermediate in the ISC process, as previously reported for other donor-acceptor BODIPY systems.[68-70] To gain more insights into the relationship between the molecular structure and the photophysical properties of distyryl-BODIPY dyads, we report here on the development of a new series of donor-acceptor type BODIPY dyads wherein the electron donor moieties are varied. Diphenylamine and carbazole donors were found to afford high fluorescence quantum yields (Φ_f ~45–75%) in polar and apolar solutions. However, negligible $^1O_2$ formation was observed for these systems. In line with our previous results for dimethylacridine, incorporation of phenoxazine and phenothiazine donors resulted in efficient PSs, with $^1O_2$ quantum yields (Φ_Δ) ranging from 33 to 47% in both chloroform and toluene solution. Fluorescence emission was quenched in chloroform for these dyads, but this feature was retained in toluene, resulting in Φ_f values around 50%. Hence, these distyryl-BODIPY dyads are interesting self-reporting PDT PSs. Femtosecond transient absorption spectroscopy (fs-TAS) was used to gain detailed insights in the excited state processes, suggesting the involvement of charge-transfer (CT) states in the ultrafast dynamics.

Results and discussion

Photosensitizer design and synthesis

The molecular design of the newly developed systems was inspired on the recently reported distyryl-BODIPY-acridine donor-acceptor (D-A) dyad **5a**, possessing both an attractive brightness and phototoxicity within the phototherapeutic window.[66] The donor end group (dimethylacridine **3a**) was deemed essential to realize exciplex formation and to allow for efficient ISC to occur. To further elucidate the origin of the ISC and the influence of the molecular design on this process, a variety of alternative donor units were now screened, going from phenoxazine (**3b**) to phenothiazine (**3c**), diphenylamine (**3d**), carbazole (**3e**), and 3,6-di-*tert*-butylcarbazole (**3f**) (Scheme 1).

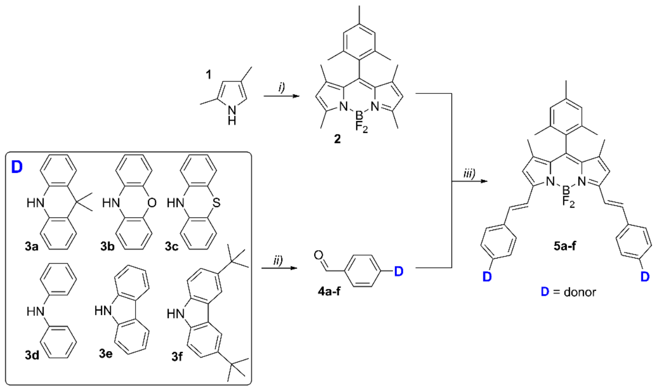

Scheme 1: Synthesis of BODIPY dyads **5a-f** and their respective building blocks: i) 2,4,6-trimethylbenzaldehyde, trifluoroacetic acid, dry CH_2Cl_2, inert atm, 3 h at 0 °C; 2,3-dichloro-5,6-dicyano-1,4-benzoquinone (DDQ), 20 min at 0 °C, 1 h at room temperature (RT); Et_3N, $BF_3{\cdot}OEt_2$, 12 h at RT (72%); ii) 4-bromobenzaldehyde, $Pd_2(dba)_3$, Cs_2CO_3, dppf, dry toluene, inert atm, 16 h at 100 °C (59–92%); iii) glacial acetic acid, piperidine, dry *N,N*-dimethylformamide (DMF), inert atm, 5 min at 150 °C (microwave irradiation) (54–91%).

For the material synthesis, donor moieties **3a-f** were first combined with 4-bromobenzaldehyde in a Buchwald-Hartwig amination reaction using tris(dibenzylideneacetone)dipalladium(0) ($Pd_2(dba)_3$) and 1,1'-bis(diphenylphosphino)ferrocene (dppf) as the catalytic system to yield aldehydes **4a-f** in moderate to high yields (59–92%). The highly fluorescent 1,3,5,7-tetramethyl-BODIPY core **2** was obtained from 2,4-dimethylpyrrole (**1**) according to a literature procedure.[71] This *meso*-mesityl-BODIPY structure was chosen for its facile synthesis and good solubility of the resulting BODIPY dyads. The relatively acidic protons of the *α*-methyl groups enable a Knoevenagel-type condensation to afford the desired distyryl-BODIPY dyads **5a-f**. A short and easy synthetic procedure, comprising five-minute microwave irradiation in the presence of glacial acetic acid and piperidine, resulted in good to high yields (54–91%). The reaction conditions were optimized previously for dimethylacridine **3a**.[66] For a detailed description of the synthesis protocols and material characterization data, we refer to the supporting information.

Structural analysis

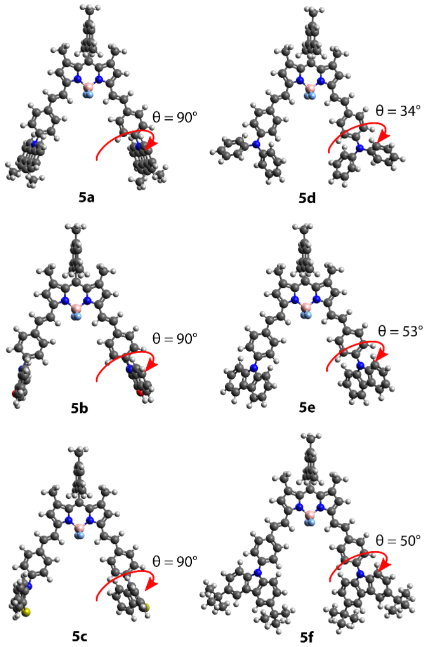

Figure 1: Optimized ground-state geometries for BODIPYs **5a-f** with the dihedral angles between the donor units and the distyryl-BODIPY core indicated by red arrows.

Density functional theory (DFT) calculations were performed to analyze the molecular structures of the BODIPY dyads with varying donor units. All geometries were optimized using the M06-2X exchange-correlation functional with the 6-311G(d) basis set and the polarizable continuum model (PCM) to simulate the moderately polar environment of a chloroform solution. Vibrational analysis was performed to confirm that all geometries correspond to minima on the potential energy surfaces. By varying the attached donor end groups in the distyryl-BODIPY dyads, large differences in the dihedral angles between the donor and acceptor moieties were observed, ranging from 34° for the diphenylamine unit (**5d**) to 90° for dimethylacridine, phenoxazine, and phenothiazine (**5a-c**) (Figure 1). This torsion angle is the same for both arms. All donor units are planar, with the exception of phenothiazine (**5c**), which is bent with an angle of 33°, and diphenylamine (**5d**), which has an angle of 70° between the two phenyl rings. The frontier molecular orbitals (Figure S1–S2) show that the highest occupied molecular orbital (HOMO) and the lowest unoccupied molecular orbital (LUMO) are located on the distyryl-BODIPY unit for **5a-f**, except for the HOMO orbital of **5b**, which is located on one of the phenoxazine units. The HOMO-1 and HOMO-2 orbitals are mainly localized on the respective donor units, again except for BODIPY **5b**, for which the HOMO-2 orbitals are located on the distyryl-BODIPY core. This discrepancy for **5b** can be explained by considering the energy levels of the various orbitals (Table S1). The quasi-degenerate HOMO-2, HOMO-1, and HOMO energies are within 0.05 eV from each other, allowing an inversion between HOMO/HOMO-1 (both localized on the donor unit) and HOMO-2 (localized on the styryl-BODIPY moiety).[72] The smaller dihedral angles in BODIPYs **5d-f** lead to increased HOMO delocalization toward the donor unit (Figure S2). In all compounds, the mesityl *meso*-group is nearly perpendicular to the rest of the BODIPY core, electronically decoupled from it.

Single crystals were obtained for BODIPYs **5a**, **5c**, and **5e** (Figure S3–S5, Table S2). The single-crystal X-ray structures confirm the molecular structures of the designed BODIPY units and also indicate that the correct geometrical conformations are probed for the time-dependent DFT (TDDFT) calculations (*vide infra*). In addition, the dihedral angles between the donor and acceptor groups were found to be 89° for **5a**, 80° for **5c**, and 70° for **5e**, which is in good agreement with the DFT calculations (Figure 1). In contrast to the findings of the DFT geometry optimization, the dimethylacridine unit is slightly bent (14°) in the single crystal structure. The bending of phenothiazine is 21° in the crystal structure, which is slightly less than observed in the geometry optimization.

TDDFT calculations

To assess the optical properties of BODIPY dyads **5a-f**, TDDFT calculations were performed using M06-2X as the exchange-correlation functional and 6-311G(d) as the basis set. The PCM was applied to simulate the solution measurement conditions in chloroform. The lowest singlet vertical excitation energies for **5a-f** are all in the region of 2.01–2.16 eV (617–573 nm) (Table 1). The second singlet vertical excitation energies are considerably larger ($\Delta E_{S1\text{-}S2}$ = 0.85–1.20 eV), making it unlikely that the S_2 states play a significant role in the photophysical properties. The two lowest triplet vertical excitation energies vary from 1.15–1.20 eV and 2.30–2.56 eV, respectively. This means that the first singlet vertical excitation energy is in between the two first triplet vertical excitation energies in all cases, as previously observed for the dimethylacridine-containing dyad **5a**.[66] BODIPY dyads **5d-f** show slightly lower first singlet and first triplet vertical excitation energies with respect to BODIPYs **5a-c**. This is likely due to the smaller dihedral angles for these donor units, resulting in delocalization of the HOMO from the BODIPY part onto the donor unit, which is not seen for BODIPYs **5a-c** (Figure S1, S2). The increase in HOMO delocalization gives rise to a more extended π-conjugated system for the transition as the first singlet excited state is of HOMO→LUMO character for all dyads, except for **5b** (HOMO-2→LUMO), for which we already denoted the inversion between the HOMO and HOMO-2 orbitals. The first singlet excited state has a large oscillator strength, which indicates high molar absorptivities (*i.e.* strong absorption).

Table 1: Calculated vertical singlet (S_1 and S_2) and triplet (T_1 and T_2) excitation energies and their corresponding oscillator strengths for BODIPYs **5a-f**. The dominant nature of the one-particle excitations is also given.

BODIPY	$S_0 \rightarrow S_1$			$S_0 \rightarrow S_2$			$S_0 \rightarrow T_1$		$S_0 \rightarrow T_2$	
	ΔE (eV)[a]	Osc. Str.[b]	Nature[c]	ΔE (eV)[a]	Osc. Str.[b]	Nature[c]	ΔE (eV)[a]	Nature[c]	ΔE (eV)[a]	Nature[c]
5a	2.16 (574 nm)	1.20	H→L (97%)	3.08	0.00	H-1→L (85%)	1.20	H→L (93%)	2.55	H-3→L (50%)
5b	2.16 (573 nm)	1.19	H-2→L (96%)	3.01	0.00	H→L (89%)	1.20	H-2→L (93%)	2.56	H-3→L (49%)
5c	2.16 (573 nm)	1.19	H→L (97%)	3.27	0.00	H-1→L (91%)	1.20	H→L (94%)	2.55	H-5→L (50%)
5d	2.01 (617 nm)	1.27	H→L (90%)	2.97	1.65	H-1→L (85%)	1.15	H→L (78%)	2.30	H-1→L (45%)
5e	2.12 (585 nm)	1.24	H→L (93%)	3.32	1.53	H-1→L (77%)	1.19	H→L (86%)	2.49	H-5→L (32%)
5f	2.11 (589 nm)	1.23	H→L (89%)	3.20	1.37	H-1→L (81%)	1.18	H→L (80%)	2.47	H-5→L (33%)

[a] Vertical excitation energy/wavelength. [b] Oscillator strength. [c] H = HOMO, L = LUMO.

To probe the CT characteristics of the push-pull BODIPY series, the ground and excited state electron densities were evaluated according to the work of Le Bahers *et al.*, using the distance over which charge is transferred (d_{CT}) and the change in dipole moment ($\Delta\mu$) as figures of merit (Table 2).[73] As the name implies, excitations with a higher degree of CT character will have larger values for d_{CT} since the charge is transferred over a certain distance as opposed to localized excitations in which the charge is merely redistributed over a given part of the molecule. Furthermore, CT excitations are characterized by a more significant $\Delta\mu$ as the charge is transferred from one part of the molecule to the other, creating areas with reduced and increased charge density distributions. For dyads **5a-f**, the $S_0 \rightarrow S_2$ transition seems to be the only excitation with CT character, as indicated by the relatively large d_{CT} (≥ 4.22 Å) and $\Delta\mu$ (≥ 18.4 D) values with respect to those for the other transitions (≤ 2.71 Å for d_{CT} and ≤ 7.2 D for $\Delta\mu$) (Table 2). As discussed before, the vertical excitation energy for the $S_0 \rightarrow S_2$ transition is much higher than for $S_0 \rightarrow S_1$ (Table 1). Hence, it seems unlikely that the S_2 state plays a significant role in the ISC process. These findings can also be visualized by considering the difference between the excited and ground state electron densities, as shown in Figure S6, S7.

Table 2: Amount of charge-transfer character (d_{CT}) and change in dipole moment ($\Delta\mu$, excited state dipole – ground state dipole) accompanying the $S_0 \rightarrow S_n$ and $S_0 \rightarrow T_n$ (n = 1,2) transitions in chloroform.

BODIPY	$S_0 \rightarrow S_1$		$S_0 \rightarrow S_2$		$S_0 \rightarrow T_1$		$S_0 \rightarrow T_2$	
	d_{CT} (Å)[a]	$\Delta\mu$ (D)[b]	d_{CT} (Å)[a]	$\Delta\mu$ (D)[b]	d_{CT} (Å)[a]	$\Delta\mu$ (D)[b]	d_{CT} (Å)[a]	$\Delta\mu$ (D)[b]
5a	0.64	1.3	5.14	34.7	0.64	1.7	0.38	0.6
5b	0.66	1.3	6.17	42.6	0.70	1.9	0.33	0.5
5c	0.59	1.2	6.11	41.8	0.64	1.7	0.28	0.5
5d	2.09	5.3	4.22	18.4	1.02	2.9	2.71	7.2
5e	1.17	2.5	4.61	20.2	0.75	2.0	1.48	2.9
5f	1.41	3.1	4.81	23.9	0.81	2.2	1.96	4.1

[a] Distance over which charge is transferred between the indicated states upon excitation. [b] Change in dipole moment upon excitation.

Photophysical characterization

The photophysical properties of the six distyryl-BODIPY dyads **5a-f** were investigated in a relatively polar (*i.e.* chloroform) and rather apolar (*i.e.* toluene) medium to explore their absorption and fluorescence behavior and their ability to generate $^1O_2$. Absorption and emission spectra afforded the basic spectral data (Figure 2, Table 3). Φ_f values were obtained at an excitation wavelength of 605 nm, relative to nile blue. Φ_Δ data were collected by monitoring the absorbance of 1,3-diphenylisobenzofuran (1,3-DPBF) as a $^1O_2$ scavenger upon excitation at 639 nm (Figure S8). In combination with the molar attenuation coefficients (ε), the brightness (*BT*) and phototoxic power (*PP*) were determined. All data reported in Table 3 are mean values from three independent measurements for each compound in the indicated solvent. Only data from the wavelength region of interest are displayed here. For the full absorption spectra, we refer to Figure S9 and Table S3.

For all BODIPY dyes, absorption maxima in chloroform were found above 630 nm, within the phototherapeutic window. Dyad **5d**, carrying the diphenylamine donor, afforded the largest bathochromic shift (190 nm) with respect to the initial BODIPY core **2**, with an absorption maximum around 690 nm. The relative positions of the absorption maxima of the different materials nicely reflect the trends in the calculated S_1 energies (Table 1). The absorption profiles resemble these of typical BODIPY dyes as they are sharp and have a high-energy absorption shoulder. The phenothiazine and diphenylamine-functionalized dyads have slightly different spectra. BODIPY **5c** shows a second, red-shifted shoulder, while the absorption band of BODIPY **5d** is clearly broadened. In the UV region, an absorption peak around 350 nm is observed in all cases, originating from the distyryl extension of the BODIPY core (Figure S9, Table S3). Other UV peaks are related to the incorporated donor. Absorption profiles in toluene solution almost entirely coincide with those in chloroform, although being slightly red-shifted (~4 nm).

As it is known that phenothiazine units can afford dual stable conformers, a relaxed potential energy surface scan was performed for compound **5c** using the M06/6-311G(d) method (Figure S10).[74] This revealed the existence of a slightly more stable conformer wherein one phenothiazine donor unit has a much smaller dihedral angle with the distyryl substituent, albeit being bent out of plane (Figure S11). This conformer is henceforth termed the 'coplanar' conformer for convenience. (TD)DFT calculations were repeated for this conformer and are presented in Table S4–S5 and Figure S12. We observed a slightly lower S_1 state compared to the perpendicular conformer (Table 1), providing a possible explanation for the presence of the red absorption shoulder for **5c** in Figure 2. Despite the larger calculated oscillator strength for the coplanar conformer, this red-shifted absorption is, however, of lower intensity. In addition, the coplanar conformer is not observed in the single-crystal structure and therefore it is considered to be less present and of little importance for the further discussion.

Table 3: Spectroscopic data for BODIPY dyads **5a-f** as obtained in chloroform and toluene solution.[a]

BODIPY	Solv.[b]	λ_{abs} (nm)[c]	λ_{em} (nm)[d]	$\Delta\bar{\nu}$ (cm^{-1})[e]	$fwhm_{abs}$ (cm^{-1})[f]	$fwhm_{em}$ (cm^{-1})[g]	ε ($M^{-1}cm^{-1}$)[h]	Φ_f[i]	Φ_Δ[j]	*BT* ($M^{-1}cm^{-1}$)[k]	*PP* ($M^{-1}cm^{-1}$)[l]
5a	CL	633	645	294	777	917	119,900	0.63±0.03	0.23±0.02	75,200	27,000
	TOL	636	649	323	744	1333	124,500	0.69±0.03	0.07±0.01	86,200	9,000
5b	CL	634	653	459	882	1165	94,800	<0.01	0.37±0.02	400	35,100
	TOL	638	663	592	884	1086	105,200	0.47±0.00	0.47±0.03	49,200	49,900
5c	CL	633	683	1156	913	987	100,400	0.05±0.00	0.38±0.01	5,500	37,900
	TOL	636	680	1017	867	777	111,600	0.53±0.00	0.33±0.01	59,600	36,900
5d	CL	687	716	589	1304	916	96,300	0.43±0.00	0.06±0.00	40,900	5,600
	TOL	691	712	427	1033	729	105,700	0.47±0.01	0.06±0.01	49,700	6,300
5e	CL	642	658	379	883	721	119,100	0.75±0.01	0.06±0.01	88,800	7,300
	TOL	647	661	339	858	659	115,700	0.73±0.02	0.04±0.03	83,900	5,100
5f	CL	648	667	440	988	773	106,100	0.70±0.01	0.02±0.01	74,200	2,000
	TOL	653	669	367	915	696	117,700	0.71±0.01	0.01±0.01	83,100	1,300

[a] All values are averaged over three independent measurements. [b] Spectrograde solvents were used for all measurements; CL = chloroform, TOL = toluene. [c] Absorption maximum. [d] Fluorescence emission maximum. [e] Energy difference between the absorption and emission maxima. [f] Full-width-at-half-maximum of the absorption band. [g] Full-width-at-half-maximum of the emission band. [h] Molar attenuation coefficient. [i] Fluorescence quantum yield determined *vs* nile blue (Φ_f = 0.27, λ_{exc} = 605 nm in spectrograde ethanol). Standard deviations are reported. [j] Singlet oxygen quantum yield determined *vs* methylene blue (Φ_Δ = 0.52, λ_{exc} = 639 nm in spectrograde ethanol) by monitoring the absorbance of 1,3-DPBF at 414 nm. Standard deviations are reported. [k] Fluorescence brightness. [l] Phototoxic power.

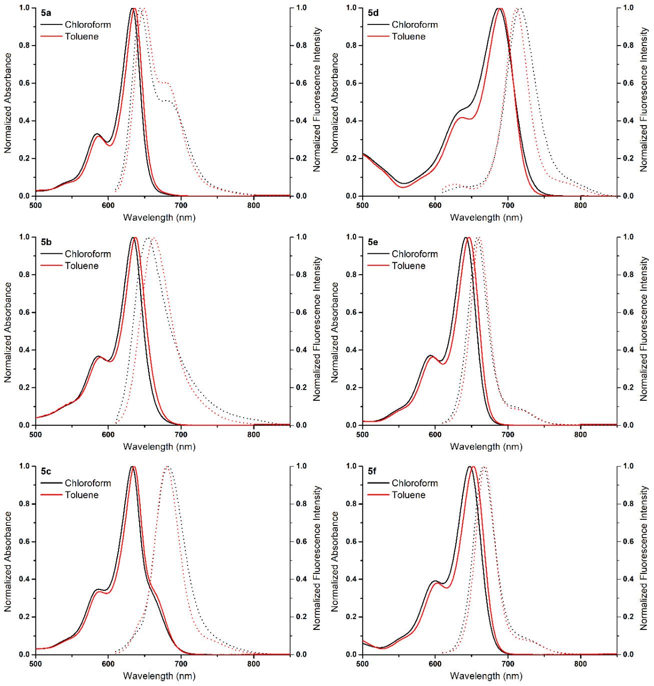

Figure 2: Normalized absorption spectra (solid lines) for BODIPYs **5a-f** and their corresponding normalized fluorescence emission spectra (dashed lines; λ_{exc} = 605 nm) in chloroform and toluene.

For the six BODIPY dyes, the emission maxima are close to their absorption counterparts, resulting in small Stokes shifts, both in chloroform and toluene solution. For phenothiazine-BODIPY dyad **5c**, the difference between the absorption and emission maxima reaches 50 nm in chloroform. This large offset is of interest for future PDT applications, since it limits interference between the activation light and the emitted fluorescence. For BODIPYs **5b,c**, only one (strongly tailing) fluorescence peak is seen. For the other donors **5a,d-f**, a low-energy emission shoulder of varying relative intensity is noticed. For a better visualization of the spectroscopic differences within the complete series, the absorption and emission profiles were plotted together in a separate figure for each solvent in Figure S13.

Φ_f and Φ_Δ values depend on the type of donor introduced and differ significantly. Generally, the fluorescence ability decreases compared to BODIPY precursor **2** (Φ_f = 0.97 in dichloromethane),[75] as expected for red-shifted dyes due to the energy-gap law. However, these values are still significant, retaining a Φ_f of at least 40% in chloroform as well as in toluene solution for dyads **5a,d-f**. The brightest variants are obtained with dimethylacridine (**5a**), carbazole (**5e**), and di-*tert*-butylcarbazole (**5f**) donors, with quantum yields around 70%. BODIPYs **5b,c** are somewhat peculiar as their emission is almost negligible in chloroform, but close to 50% in toluene. According to Φ_Δ, we can divide the six dyads into two groups, in line with our observations on the D-A dihedral angles given in Figure 1. The BODIPY materials based on diphenylamine and both carbazole donors (**5d-f**; $\theta_{D\text{-}A} < 90°$) are unable to produce a considerable amount of $^1O_2$ during excitation at 639 nm (around or below 6%). On the other hand, dimethylacridine, phenoxazine, and phenothiazine (**5a-c**; $\theta_{D\text{-}A} = 90°$) afford suitable PSs with $^1O_2$ quantum yields of 23, 37, and 38% in chloroform, respectively. The Φ_Δ value for the dimethylacridine-based dyad **5a** in toluene drops below 10%. Interestingly, this is not the case for phenoxazine and phenothiazine dyads **5b-c**, where $^1O_2$ production is still significant, with yields of 47 and 33%, respectively. Hence, the combination of strong fluorescence and $^1O_2$ formation, together with their high molar attenuation coefficients, renders these new distyryl-BODIPY dyes promising dual-functioning PSs.

Concentration-dependent fluorescence

At this stage, the underlying mechanism explaining the differences in Φ_Δ remains unclear. TDDFT calculations (Table 2) showed that ISC *via* intermediate CT states (SOCT-ISC), as often proposed in literature for push-pull type (BODIPY) dyes, seems unlikely as there is no available CT state.[40-42, 47, 48] In our previous work on BODIPY-dimethylacridine dyads (**5a**), we suggested that ISC could possibly proceed *via* an exciplex intermediate state (^{1}EX).[66] Hence, a similar screening of the fluorescence profile at different concentrations was performed for BODIPYs **5b-f** (Figure 3, S14-S16).

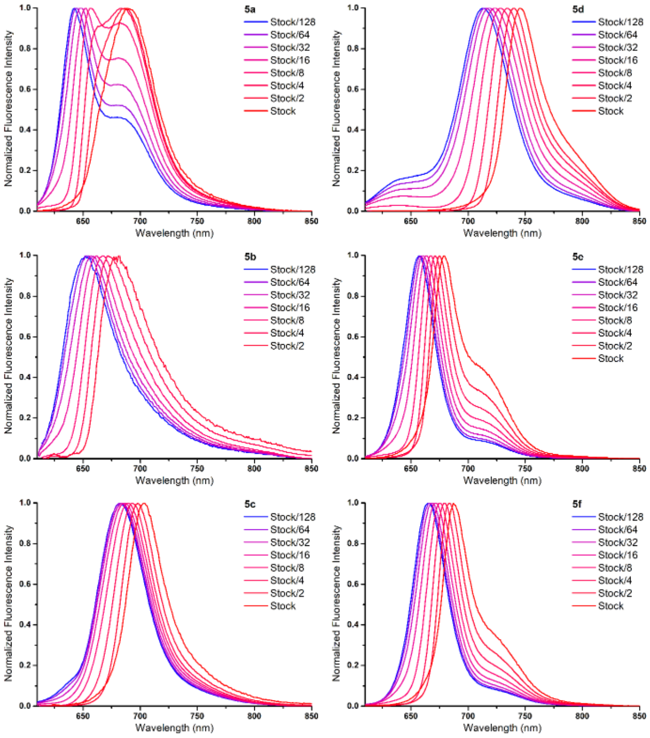

Figure 3: Normalized fluorescence emission spectra for a dilution series of BODIPYs **5a-f** in chloroform (λ_{exc} = 605 nm). Stock solutions contained ca. 1 mg BODIPY in 5 mL chloroform.

A bathochromic shift in the fluorescence maxima was observed for the six BODIPYs upon increasing concentration. This is a commonly observed phenomenon, whereby the increased molecular interaction enlarges the perceived Stokes shift.[76] As previously described, dyad **5a** shows a strong increase in relative intensity of a second emission band as the concentration increases.[66] In diluted samples, the localized singlet state (^{1}LE) emission at 645 nm is most intense. As concentration increases, the relative population of the ^{1}LE and ^{1}EX band is altered, and the exciplex state becomes more distinct. This trend results in an exciplex band ($\lambda_{em,EX}$ = 690 nm) that transcends the ^{1}LE emission. In the stock solution, the ^{1}LE emission even disappeared completely, with only the emission from the

^{1}EX state remaining. Similar behavior is observed in toluene (Figure S14). For the other dyads (**5b-f**), this remarkable behavior is not explicitly visible (Figure 3, S14). A slight increase of the long-wavelength fluorescence shoulder can be noticed for BODIPYs **5d-f** upon increasing concentration, but not at all to the same extent as for **5a**. Furthermore, the dyads with phenoxazine and phenothiazine donors (**5b-c**) do not show a second emission band resulting from molecular aggregation, despite their ISC ability. Hence, exciplex formation seems to occur only for dyad **5a**, whereas BODIPYs **5b-c** have to rely on another mechanism to explain their high $^{1}O_2$ generation capabilities upon photoexcitation. To get a better idea of the relative fluorescence intensities at different concentrations, these data were also normalized to the concentration (Figure S15, S16). In all cases, a strong quenching of the emissive behavior was observed upon increasing concentration.

Femtosecond transient absorption spectroscopy

Transient absorption spectra, recorded with a high time resolution of ~30 fs, were measured to gain additional information on the ultrafast excited state evolutions of the dyads. All samples were excited using a broadband ultrashort pulse (<30 fs) covering the 550–760 nm spectral range. A second broadband ultrashort pulse was used as the probe beam. Transient spectra were acquired within a pump-probe time delay window of 200 ps. The raw transient absorption spectra are shown in Figure S17–S18. To extract the time constants associated with the excited state evolution, a global fitting of the kinetic traces was performed using a sequential linear kinetic scheme (using the software Glotaran).[77] The evolution-associated difference spectra (EADS) obtained from global analysis for BODIPYs **5a-f** in toluene solution are reported in Figure 4. Global analysis was also performed on the transient data of dyads **5a-f** in chloroform solution. The EADS are very similar to those obtained in toluene solution, although there are small differences in the extracted kinetic constants (Figure S19).

To facilitate the analysis, a reference compound lacking a donor moiety (distyryl-BODIPY **5H**, Donor = H in Scheme 1) was synthesized and transient spectra were acquired for this compound as well (Figure S20). The initial EADS of the reference compound presents an intense negative band peaked at 620 nm, assigned to ground-state bleaching (GSB). Furthermore, a low-intensity excited-state absorption (ESA) and a stimulated emission (SE) band, respectively peaked at 648 and 684 nm, are also observed (Figure S20). This spectral component evolves toward the second EADS in 260 fs. The spectral difference among the two initial EADS is very small, and this transition can be interpreted as a fast electronic relaxation of the excited state. The second component further evolves in 48.5 ps toward the final EADS. During this evolution, the intensity of the bleaching signal decreases and its maximum red-shifts slightly. At the same time, the ESA and SE bands also red-shift, although their intensity remains almost unvaried. Considering the timescale of this evolution, the most likely interpretation for the observed spectral changes is a structural relaxation occurring in the excited state, possibly involving a partial rotation of the phenyl substituents. The lifetime of the final spectral component is estimated by the analysis as 200 ps. This value is affected by a significant error, as the longest time delay accessed within the measurements is also 200 ps. Because of its strong fluorescence (Φ_f = 0.98 in toluene), it is expected that the effective lifetime of S_1 would be in the order of a few nanoseconds.

Commentato [MDD1]: If shortening is necessary this paragraph can be moved to SI

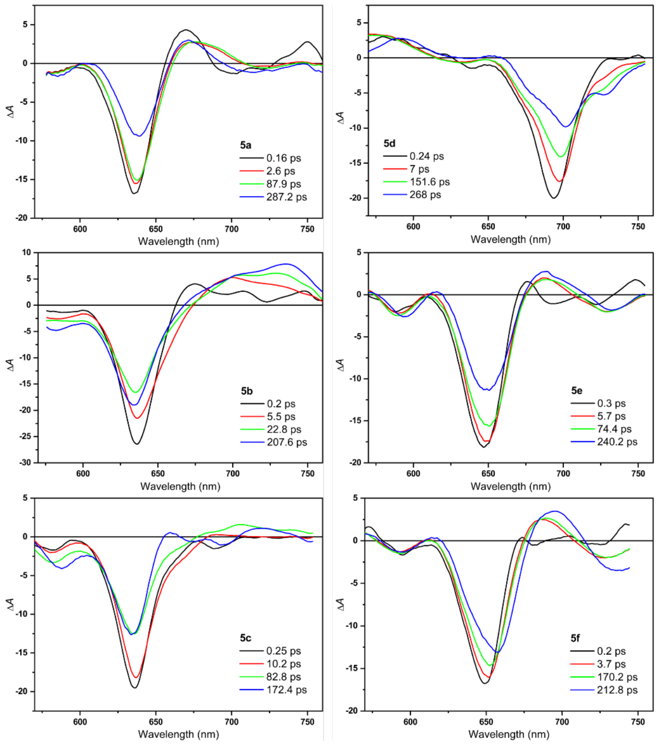

Figure 4: Evolution-associated difference spectra (EADS) for BODIPYs **5a-f** in toluene solution as obtained by singular value decomposition (SVD) and global fitting of the transient data (target analysis).

Considering the newly synthesized dyads **5a-f**, whose EADS are reported in Figure 4, the most intense signal is a negative band whose position matches well with the absorption maximum (Figure 2) and can thus be assigned to GSB. Besides, differences are observed for the smaller intensity ESA and SE bands. As noticed in Figure 4, the EADS of BODIPYs **5b,c** are qualitatively similar. In both cases, a positive band is observed to rise on a 10–20 ps timescale in the 680–750 nm region, while the low intensity SE band is not observed for these systems. In case of phenoxazine-BODIPY **5b**, the positive signal starts rising at the short timescale since it is already observed in the second spectral component, with a rise time of 200 fs. The positive band is initially peaked at 700 nm. Within the following 5.5 ps, the ESA intensity increases and a second maximum at 730 nm appears. The band further rises in the evolution toward the following EADS, occurring in 23 ps. The intensity of the bleaching signal progressively recovers, and its peak slightly blue-shifts in time. For phenothiazine-BODIPY **5c**, the rise of the positive band appears slower as compared to **5b**. Indeed, a positive band peaked at 700 nm is clearly observed only in the third spectral component, rising in 10 ps. In the following EADS, a negative signal appears in the 660–700 nm region, while two positive peaks are visible at 650 and 710 nm. The appearance of a positive band on the red side of the bleaching band can point to the occurrence of charge separation between the BODIPY core and the donor substituents. Indeed, it was previously indicated that the localization of a negative charge on a BODIPY core induces the appearance of an absorption band on the red side of the GSB of the correspondent neutral species.[64] The spectral evolution observed for dyad **5c** on the 83 ps timescale could point to a structural relaxation of the charge-separated state (CSS).

The occurrence of charge separation is less clear in case of BODIPY **5a**. The transient spectra registered in the two solvents are very similar (Figure 4, S19). The initial EADS resembles that of the distyryl BODIPY without a donor moiety (**5H**; Figure S20). The signal evolves in 160 fs, with the ESA band broadening and compensating the SE band. The spectral shape remains almost unvaried in the following evolution (2.6 ps), while in the subsequent evolution (88 ps) both the GSB and ESA band decrease in intensity. A small SE signal is again visible in the final spectral component because of the decreased intensity of the positive signal in the same region. The rise of a positive signal in the 700 nm region could indicate the presence of a CSS. However, the kinetics of this process are different compared to what was observed for BODIPYs **5b,c**. Comparing the kinetic traces recorded on the ESA band of compounds **5a-c** (Figure S21), it can be noticed that the positive band in **5b,c** rises on a similar timescale of a few tens of ps, while the rise for **5a** is much faster and is followed by a faster decay. Comparison of the transient absorption data thus suggests that the ISC mechanism for these dyes might be different, with triplet formation possibly mediated by the presence of exciplexes in case of dimethylacridine-BODIPY **5a** and charge separation/recombination for phenoxazine- and phenothiazine-BODIPYs **5b,c**.

The EADS of BODIPYs **5d-f** are qualitatively different from those of BODIPYs **5a-c** (Figure 4, S19). In particular, the EADS of carbazole-BODIPYs **5e,f** closely resemble those of the distyryl-BODIPY **5H**, although red-shifted. The ESAs observed in these compounds, peaked at 688 and 700 nm, respectively, have a very fast rise, suggesting that this signal is associated to the bright S_1 state. This is clearly shown by the comparison of the kinetic traces recorded on the ESAs of **5b** and **5f** shown in Figure S22. The spectra of diphenylamine-BODIPY **5d** are different, reflecting the strong red-shift in the absorption observed for this sample. Indeed, in this case, the bleaching signal is located at 693 nm and an ESA band is observed in the blue part of the investigated spectral region (560 nm). Following the time evolution, the bleaching progressively recovers, while a SE band appears around 730 nm. This band progressively increases in intensity and slightly red-shifts, signaling the occurrence of emission by a relaxed excited state. Nevertheless, also in this case there is no indication of the involvement of other excited states in the dynamics, which thus proceeds through relaxation from the bright S_1 state.

To gain further information on the occurring of charge separation and on the differences observed in case of samples **5a-c** as compared to samples **5d-f,** the transient spectra of two representative compounds for each group, namely **5b** and **5e** have been measured on an extended timescale reaching 1.5 ns pump-probe delay in both toluene and chloroform. The EADS obtained by performing a global analysis on these data are reported in SI (see Figure **SX** and **SY** and related additional comments). As it can be clearly noticed by inspection of the EADS, the excited state dynamics on the timescale >200 ps is highly influenced by the solvent polarity in case of sample **5b**, as expected in case of charge separation. Indeed the transient spectra recover almost completely within the inspected 1.5 ns timescale in chloroform, suggesting the occurrence of charge recombination, while a slower dynamics is observed in toluene. In case of sample **5e** both the spectral shape and the signal evolution are almost independent on the solvent polarity.

Excited state geometry optimizations

Since the femtosecond transient absorption spectra suggest the presence of an intermediate state with CT character in BODIPY dyads **5b,c** (Figure 4), whereas there is no evidence of the involvement of this state from TDDFT calculations on the ground state geometry (Table 2), excited state geometry optimizations were performed to probe the effects of geometrical relaxation. Using the same level of approximation as applied for the ground state optimizations (M062X/6-311G(d)), the excited state geometries for the first (LE character) and second (CT character) excited states were optimized in the gas phase. Upon relaxation, the first singlet excited states of BODIPYs **5a,b** show smaller D-A dihedral angles of 82° and 64°, respectively (Figure S23-S24). For BODIPY **5c**, this is not the case (Figure S25). BODIPYs **5d-f** do not show significant differences in the D-A dihedral angles as compared to the ground states either (Figure S26-S28). The decrease in dihedral angle for **5a,b** leads to a delocalization of the

HOMO onto the donor and distyryl-BODIPY fragments and mixes CT and LE character for the first singlet excited state (Figure S23-S24, Table S6). For **5b**, this effect is much stronger due to the strongly reduced dihedral angle with respect to the ground state geometry. When optimizing the second singlet excited state, the D-A dihedral angles remain unchanged as compared to the ground state (Figure S23–S28). The S_1-S_2 energy difference ($\Delta E_{S1\text{-}S2}$) remains unchanged for BODIPYs **5d-f** and no mixing of CT and LE character is observed for these molecules. However, a strong decrease of $\Delta E_{S1\text{-}S2}$ is observed for BODIPYs **5a** and (in particular) **5b**, indicating that the excited states are close in energy for this given geometry (Table S7). For dyad **5c**, we were unable to optimize the second singlet excited state due to a rearrangement of the energy levels during the optimization procedure. We do observe that the vertical de-excitation energies of S_1 and S_2 come very close and even invert before the energy level rearrangement occurs. These results indicate that after excited state relaxation, the LE and CT excited state come closer in energy for BODIPYs **5b,c** thus enabling a mixing between them. This is in line with the findings of the femtosecond transient absorption experiments and further solidifies the hypothesis that a CT state is involved in the ISC process.

Involvement of CT states also allows to clarify the strong solvent dependence of the fluorescence intensity of **5b,c** (Table 3). As CT states are highly polar excited states, their energy is strongly affected by the surrounding medium.[78] In a more polar solvent (*e.g.* chloroform), the CT state is stabilized, thereby decreasing its energy. However, the approach of the CT state to the ground state induces more radiationless relaxation. Accordingly, dyads **5b,c** show quenched emission in chloroform. In relatively apolar toluene solution, a larger singlet state population is retained, preserving the fluorescence.

Conclusions

A series of six different distyryl-BODIPY-donor dyads were synthesized and the photophysical properties were evaluated with an eye on their potential application as photosensitizers in image-guided photodynamic therapy. All dyes show strong absorption in the phototherapeutic window. The main differences are found in their brightness and phototoxic behavior. BODIPYs bearing diphenylamine or carbazole donors show moderate to strong fluorescence, respectively, but produce very little singlet oxygen upon photoexcitation. Dimethylacridine, phenoxazine, and phenothiazine donors are oriented perpendicularly with respect to the styryl moieties in the ground state geometry. This seems to be an essential structural feature as, next to a moderate fluorescence quantum yield, these dyads afford significant singlet oxygen quantum yields without the aid of heavy atoms. Phenoxazine- and phenothiazine-bearing BODIPYs show improved photosensitizer characteristics with respect to the earlier reported dimethylacridine-distyryl BODIPY dyads. With Φ_f = 53% and Φ_Δ = 33% for phenothiazine, and $\Phi_f = \Phi_\Delta$ = 47% for phenoxazine (in toluene), these new dyads can be considered as highly promising dual-functioning photosensitizers. The intersystem crossing mechanism in the BODIPY dyads was studied using femtosecond transient absorption spectroscopy. Charge separation/recombination seems to take place in the phenoxazine- and phenothiazine-based molecules. This hypothesis was further solidified by optimizing the first and second excited state geometries, revealing their relatively small energy difference, allowing mixing between them. Due to these promising results, steps will be taken now to probe the behavior of the novel photosensitizers in biological media with an eye on future *in vitro* and *in vivo* examinations.

Conflict of interest

There are no conflicts of interest to declare.

Acknowledgments

The authors thank Hasselt University and the University of Namur for continuing financial support (Ph.D. scholarships JD and TC). BC and WM thank the Research Foundation – Flanders (FWO) for support through projects G087718N, G0D1521N, I006320N, GOH3816NAUHL, and the Scientific

Research Community 'Supramolecular Chemistry and Materials' (W000620N). The calculations were performed on the computers of the 'Consortium des équipements de Calcul Intensif (CÉCI)' (http://www.ceci-hpc.be), including those of the 'UNamur Technological Platform of High-Performance Computing (PTCI)' (http://www.ptci.unamur.be), for which we gratefully acknowledge financial support from the FNRS-FRFC, the Walloon Region, and the University of Namur (Conventions No. 2.5020.11, GEQ U.G006.15, U.G018.19, 1610468, and RW/GEQ2016). SD, AL, and MDD acknowledge support from the European Union's Horizon 2020 research and innovation program under grant agreement n. 871124 Laserlab-Europe.

Supporting information

Materials and methods, detailed BODIPY dyad synthesis procedures and characterization data, additional (TD)DFT data and figures, single-crystal X-ray structures, singlet oxygen generation plots, additional absorption and emission spectra and data, additional transient absorption spectra and data, and $^{1}H/^{13}C$ NMR spectra can be found in the supporting information.

Keywords

BODIPY • Photosensitizer • Near-Infrared • Heavy-Atom-Free • Intersystem Crossing • Theranostics

References

1. M. C. DeRosa and R. J. Crutchley, *Coordin. Chem. Rev.*, 2002, **233**, 351-371.
2. J. Moan, *J. Photochem. Photobiol. B*, 1990, **6**, 343-347.
3. J. Moan and K. Berg, *Photochem. Photobiol.*, 1991, **53**, 549-553.
4. S. Kwiatkowski, B. Knap, D. Przystupski, J. Saczko, E. Kedzierska, K. Knap-Czop, J. Kotlinska, O. Michel, K. Kotowski and J. Kulbacka, *Biomed. Pharmacother.*, 2018, **106**, 1098-1107.
5. H. I. Pass, *J. Natl. Cancer Inst.*, 1993, **85**, 443-456.
6. W. M. Sharman, C. M. Allen and J. E. van Lier, *Drug Discovery Today*, 1999, **4**, 507-517.
7. T. J. Dougherty, *J. Clin. Laser Med. Sur.*, 2002, **20**, 3-7.
8. M. R. Hamblin and T. Hasan, *Photochem. Photobiol. Sci.*, 2004, **3**, 436-450.
9. Z. Huang, *Technol. Cancer Res. Treat.*, 2005, **4**, 283-293.
10. M. A. MacCormack, *Semin. Cutan. Med. Surg.*, 2008, **27**, 52-62.
11. P. Babilas, S. Schreml, M. Landthaler and R. M. Szeimies, *Photodermatol. Photoimmunol. Photomed.*, 2010, **26**, 118-132.
12. T. Dai, B. B. Fuchs, J. J. Coleman, R. A. Prates, C. Astrakas, T. G. St Denis, M. S. Ribeiro, E. Mylonakis, M. R. Hamblin and G. P. Tegos, *Front. Microbiol.*, 2012, **3**, 120-136.
13. C. S. Foote, *Photochem. Photobiol.*, 1991, **54**, 659-659.
14. A. P. Castano, T. N. Demidova and M. R. Hamblin, *Photodiagn. Photodyn. Ther.*, 2004, **1**, 279-293.
15. V. Kral, J. Davis, A. Andrievsky, J. Kralova, A. Synytsya, P. Pouckova and J. L. Sessler, *J. Med. Chem.*, 2002, **45**, 1073-1078.
16. S. J. Wagner, *Transfus. Med. Rev.*, 2002, **16**, 61-66.
17. R. R. Allison, G. H. Downie, R. Cuenca, X. H. Hu, C. J. Childs and C. H. Sibata, *Photodiagn. Photodyn. Ther.*, 2004, **1**, 27-42.
18. M. R. Detty, S. L. Gibson and S. J. Wagner, *J. Med. Chem.*, 2004, **47**, 3897-3915.
19. A. E. O'Connor, W. M. Gallagher and A. T. Byrne, *Photochem. Photobiol.*, 2009, **85**, 1053-1074.
20. S. Swavey and M. Tran, in *Recent Advances in the Biology, Therapy and Management of Melanoma*, ed. L. Davids, IntechOpen, London, 2013, ch. 11, pp. 254-282.
21. R. D. Teo, J. Y. Hwang, J. Termini, Z. Gross and H. B. Gray, *Chem. Rev.*, 2017, **117**, 2711-2729.
22. S. D'Alessandro and R. Priefer, *J. Drug Deliv. Sci. Tec.*, 2020, **60**, 101979.
23. J. Deckers, T. Cardeynaels, L. Lutsen, B. Champagne and W. Maes, *ChemPhysChem*, 2021, **22**, 1488-1496.
24. S. G. Awuah and Y. You, *RSC Adv.*, 2012, **2**, 11169-11183.
25. L. Yao, S. Z. Xiao and F. J. Dan, *J. Chem.*, 2013, **2013**, 1-10.
26. A. Kamkaew, S. H. Lim, H. B. Lee, L. V. Kiew, L. Y. Chung and K. Burgess, *Chem. Soc. Rev.*, 2013, **42**, 77-88.
27. C. S. Kue, S. Y. Ng, S. H. Voon, A. Kamkaew, L. Y. Chung, L. V. Kiew and H. B. Lee, *Photochem. Photobiol. Sci.*, 2018, **17**, 1691-1708.
28. L. Huang and G. Han, *Small Methods*, 2018, **2**, 1700370.
29. A. Turksoy, D. Yildiz and E. U. Akkaya, *Coordin. Chem. Rev.*, 2019, **379**, 47-64.
30. W. Sun, X. Zhao, J. Fan, J. Du and X. Peng, *Small*, 2019, **15**, 1804927.

31. M. L. Agazzi, M. B. Ballatore, A. M. Durantini, E. N. Durantini and A. C. Tomé, *J. Photochem. Photobiol. C*, 2019, **40**, 21-48.
32. D. Chen, Z. Zhong, Q. Ma, J. Shao, W. Huang and X. Dong, *ACS Appl. Mater. Interfaces*, 2020, **12**, 26914-26925.
33. P. Chinna Ayya Swamy, G. Sivaraman, R. N. Priyanka, S. O. Raja, K. Ponnuvel, J. Shanmugpriya and A. Gulyani, *Coordin. Chem. Rev.*, 2020, **411**, 213233.
34. W. Lin, D. Colombani-Garay, L. Huang, C. Duan and G. Han, *WIREs Nanomed. Nanobiotechnol.*, 2020, **12**, 1627.
35. R. Prieto-Montero, A. Prieto-Castañeda, R. Sola-Llano, A. R. Agarrabeitia, D. Garcia-Fresnadillo, I. López-Arbeloa, A. Villanueva, M. J. Ortiz, S. de la Moya and V. Martínez-Martínez, *Photochem. Photobiol.*, 2020, **96**, 458-477.
36. W. Zhang, A. Ahmed, H. Cong, S. Wang, Y. Shen and B. Yu, *Dyes Pigments*, 2021, **185**, 108937.
37. A. Loudet and K. Burgess, *Chem. Rev.*, 2007, **107**, 4891-4932.
38. G. Ulrich, R. Ziessel and A. Harriman, *Angew. Chem. Int. Ed.*, 2008, **47**, 1184-1201.
39. N. Boens, B. Verbelen and W. Dehaen, *Eur. J. Org. Chem.*, 2015, **2015**, 6577-6595.
40. J. Zhao, K. Xu, W. Yang, Z. Wang and F. Zhong, *Chem. Soc. Rev.*, 2015, **44**, 8904-8939.
41. K. Chen, Y. Dong, X. Zhao, M. Imran, G. Tang, J. Zhao and Q. Liu, *Front. Chem.*, 2019, **7**, 1-14.
42. J. Wang, Q. B. Gong, L. Wang, E. H. Hao and L. J. Jiao, *J. Porph. Phthalocyanines*, 2020, **24**, 603-635.
43. G. Kubheka, B. Babu, E. Prinsloo, N. Kobayashi, J. Mack and T. Nyokong, *J. Porph. Phthalocyanines*, 2020, **25**, 47-55.
44. J. Zhao, W. Wu, J. Sun and S. Guo, *Chem. Soc. Rev.*, 2013, **42**, 5323-5351.
45. J. Zhao, K. Chen, Y. Hou, Y. Che, L. Liu and D. Jia, *Org. Biomol. Chem.*, 2018, **16**, 3692-3701.
46. Y. Hou, X. Zhang, K. Chen, D. Liu, Z. Wang, Q. Liu, J. Zhao and A. Barbon, *J. Mater. Chem. C*, 2019, **7**, 12048-12074.
47. M. A. Filatov, *Org. Biomol. Chem.*, 2020, **18**, 10-27.
48. V. N. Nguyen, Y. Yan, J. Zhao and J. Yoon, *Acc. Chem. Res.*, 2021, **54**, 207-220.
49. J. P. Celli, B. Q. Spring, I. Rizvi, C. L. Evans, K. S. Samkoe, S. Verma, B. W. Pogue and T. Hasan, *Chem. Rev.*, 2010, **110**, 2795-2838.
50. S. S. Kelkar and T. M. Reineke, *Bioconjugate Chem.*, 2011, **22**, 1879-1903.
51. X. Chen and S. T. C. Wong, *Cancer Theranostics*, Academic Press, Oxford, 2014.
52. T. J. Dougherty and S. L. Marcus, *Eur. J. Cancer*, 1992, **28**, 1734-1742.
53. K. Plaetzer, B. Krammer, J. Berlanda, F. Berr and T. Kiesslich, *Lasers Med. Sci.*, 2009, **24**, 259-268.
54. K. Deng, C. Li, S. Huang, B. Xing, D. Jin, Q. Zeng, Z. Hou and J. Lin, *Small*, 2017, **13**, 1702299.
55. A. B. Descalzo, H. J. Xu, Z. Shen and K. Rurack, *Ann. N. Y. Acad. Sci.*, 2008, **1130**, 164-171.
56. L. Yuan, W. Lin, K. Zheng, L. He and W. Huang, *Chem. Soc. Rev.*, 2013, **42**, 622-661.
57. Y. Ni and J. Wu, *Org. Biomol. Chem.*, 2014, **12**, 3774-3791.
58. H. Lu, J. Mack, Y. Yang and Z. Shen, *Chem. Soc. Rev.*, 2014, **43**, 4778-4823.
59. S. G. Awuah, S. K. Das, F. D'Souza and Y. You, *Chem. Asian J.*, 2013, **8**, 3123-3132.
60. R. L. Watley, S. G. Awuah, M. Bio, R. Cantu, H. B. Gobeze, V. N. Nesterov, S. K. Das, F. D'Souza and Y. You, *Chem. Asian J.*, 2015, **10**, 1335-1343.
61. Z. Wang, L. Huang, Y. Yan, A. M. El-Zohry, A. Toffoletti, J. Zhao, A. Barbon, B. Dick, O. F. Mohammed and G. Han, *Angew. Chem. Int. Ed.*, 2020, **59**, 16114-16121.
62. H. Ito, H. Sakai, Y. Suzuki, J. Kawamata and T. Hasobe, *Chem. Eur. J.*, 2020, **26**, 316-325.
63. Y. Hou, Q. Liu and J. Zhao, *Chem. Commun.*, 2020, **56**, 1721-1724.
64. Y. Dong, A. Elmali, J. Zhao, B. Dick and A. Karatay, *ChemPhysChem*, 2020, **21**, 1388-1401.
65. G. Turkoglu, G. Kayadibi Koygun, M. N. Z. Yurt, N. Demirok and S. Erbas-Cakmak, *Org. Biomol. Chem.*, 2020, **18**, 9433-9437.
66. J. Deckers, T. Cardeynaels, H. Penxten, A. Ethirajan, M. Ameloot, M. Kruk, B. Champagne and W. Maes, *Chem. Eur. J.*, 2020, **26**, 15212-15225.

67. As the exact structure of these 'exciplexes' (*i.e.* excited state complexes) remains unknown for now, we propose to use this more general term.
68. A. C. Benniston, G. Copley, H. Lemmetyinen and N. V. Tkachenko, *ChemPhysChem*, 2010, **11**, 1685-1692.
69. A. C. Benniston, A. Harriman, V. L. Whittle, M. Zelzer, R. W. Harrington and W. Clegg, *Photochem. Photobiol. Sci.*, 2010, **9**, 1009-1017.
70. A. Nano, R. Ziessel, P. Stachelek, M. A. Alamiry and A. Harriman, *ChemPhysChem*, 2014, **15**, 177-186.
71. Y. Rong, C. Wu, J. Yu, X. Zhang, F. Ye, M. Zeigler, M. E. Gallina, I. C. Wu, Y. Zhang, Y. H. Chan, W. Sun, K. Uvdal and D. T. Chiu, *ACS Nano*, 2013, **7**, 376-384.
72. H. Y. Yang, M. Zhang, J. W. Zhao, C. P. Pu, H. Lin, S. L. Tao, C. J. Zheng and X. H. Zhang, *Chin. J. Chem.*, 2021, **39**.
73. T. Le Bahers, C. Adamo and I. Ciofini, *J. Chem. Theory Comput.*, 2011, **7**, 2498-2506.
74. K. Wang, Y. Z. Shi, C. J. Zheng, W. Liu, K. Liang, X. Li, M. Zhang, H. Lin, S. L. Tao, C. S. Lee, X. M. Ou and X. H. Zhang, *ACS Appl. Mater. Interfaces*, 2018, **10**, 31515-31525.
75. A. B. Nepomnyashchii, M. Broring, J. Ahrens and A. J. Bard, *J. Am. Chem. Soc.*, 2011, **133**, 8633-8645.
76. J. R. Lakowicz, *Principles of Fluorescence Spectroscopy*, Springer, Boston, MA, 3 edn., 2006.
77. J. J. Snellenburg, S. P. Laptenok, R. Seger, K. M. Mullen and I. H. M. v. Stokkum, *J. Stat. Soft.*, 2012, **49**, 1-22.
78. D. Escudero, *Acc. Chem. Res.*, 2016, **49**, 1816-1824.